Available online at www.sciencedirect.com
SCIENCE DIRECT
Mathematical and Computer Modelling 43 (2006) 1275–1287
MATHEMATICAL AND COMPUTER MODELLING
www.elsevier.com/locate/mcm

CFD study of section characteristics of Formula Mazda race car wings

W. Kieffer[a], S. Moujaes[b,*], N. Armbya[b]

[a] *MSME UNLV 2002, United States*
[b] *ME Department, UNLV, United States*

Received 2 November 2004; received in revised form 14 March 2005; accepted 21 March 2005

Abstract

A great deal of research has been done on the aerodynamic characteristics of race cars competing in major racing series through out the world. Because of the competitive nature of motor sport, this research is usually not published until after it is obsolete. The teams operating at the minor league levels of the sport do not have the funding resources of the major series to perform aerodynamic research. In an effort to provide some information for teams competing in the minor league Formula Mazda racecar class, this study was conducted using the Star-CD CFD code to perform a turbulent simulation (using a k–ε model) of the airflow on the front and rear wings of a Formula Mazda car with different angles of attack and the effect of the ground on the front wing. Results are presented graphically, showing pressure and velocity distributions and lift (C_l) and drag coefficients (C_d) for the different cases. It was shown that the ground effect has a marked effect on the C_l and that the angle of attack has a significant effect on the lift and drag coefficients, and it was shown that an angle of 12° below the horizontal seems to indicate stalling conditions. It is suggested that this information, along with experimental validation, can be valuable for improving the optimum handling of these Formula Mazda race cars.

Keywords: CFD; Aerofoil; Mazda race cars; k–ε turbulent modelling

1. Introduction

Aerodynamic developments that result from research in the highly competitive environment of motor sport are used as a competitive advantage for the team or manufacturer that funded the research. Any team that gains an advantage is rather reluctant to share that information with their competitors. Therefore, much of the research in this industry/sport is not published. The research that is published refers to generic shapes or to vehicles that are no longer competitive due to rule changes or other technological developments.

The work by [1] contains theoretical fundamentals of the flow across two-dimensional (2-D) wing sections and the application of the theories to three dimensions (3-D). Research in [2] investigated the design and effectiveness of

* Corresponding address: University of Nevada Las Vegas, Department of Mechanical Engineering, 4505 Maryland PkwyBox 454027, 89154-4027 Las Vegas, NV, United States.
E-mail address: samir@me.unlv.edu (S. Moujaes).

0895-7177/$ - see front matter © 2005 Elsevier Ltd. All rights reserved.
doi:10.1016/j.mcm.2005.03.011

Fig. 1. Formula Mazda race car.

airfoils for high lift in subsonic conditions. Liebeck also investigated the effects of the Gurney flap, which is a flat plate located normal to the chord line at the airfoil trailing edge and can have some effect on the local hydrodynamics of the wing [3], and extended Abbott's work to develop his own series of airfoils for a variety of purposes. A portion of his work involved airfoils for high lift, and low Reynolds number conditions [4]. He performed tests in the Langley water tunnel on wings with different Gurney flap configurations to investigate visually the flow field near a Gurney flap. It was found that the flow field theorized by Liebeck was generally substantiated for the different Gurney flap geometries considered in [5]. Liebeck's study investigated the effect of wing/body interaction on two generic shapes of closed-wheel racecars. They then combined three-dimensional computer simulation techniques with wind tunnel testing during the aerodynamic development of a closed-wheel race car (1994) [6], performed experimental and computational studies of a two-dimensional airfoil in ground effect [7], and performed experimental tests on a variety of airfoil configurations in the Wichita State University Beech Memorial low-speed wind tunnel.

As was mentioned in the literature review, much of the published research in the motor-sports industry is based on generic shapes or obsolete equipment. The research is geared towards race cars competing in the major racing series throughout the world, where there is a greater value return for the research. The significance of this study is that it provides aerodynamic characteristics for a particular class of currently legal race cars operated in amateur and minor level auto racing series where this information is lacking. The subject of this paper is a study of the aerodynamic characteristics of the wings on a Formula Mazda racecar. Two wing profile (front and back), angle of attack, and the lift and drag characteristics of these wings will be studied. This study will be a turbulent Reynolds number flow using a k–ε model in a numerical simulation of the aerodynamic effects of different angles of attack for the front and rear wings of a Formula Mazda race car. For the effect of the ground on the front wing, a new result will be presented for the front airfoil used in this class of race cars.

2. General description of Formula Mazda car

The Formula Mazda racing class was designed as a low cost, lower level series with an emphasis on driver development. As such, changes to the design of the chassis, bodywork and engine are prohibited. An example of a Formula Mazda racecar is shown in Fig. 1. This particular car belongs to the Bullet Racing Team of San Clemente, California. It is a single seat, open-wheel racecar equipped with racing slick tires. A slightly modified Mazda 13B rotary engine is connected to a 5-speed transaxle with a specified list of approved gear ratios. Water and oil coolers are specified along with the size of the cooling air inlet and outlet openings. The bodywork is a non-ground effect flat bottom with front and rear wings. The SCCA, Inc. rules, 2002, limit the wing plan form and cross sectional profile to that provided by the manufacturer. The angle of attack is adjustable to a maximum of $+16^\circ$, measured from the top of the center section of the wing to the top of the trailing edge. This is a departure from the normal practice in the field of aerodynamics of referencing the angle of attack from a line drawn between the centers of the leading edge and the trailing edge. The method used by the SCCA, Inc. allows for easier and quicker measurement, using simple tools at the racetrack, to ensure compliance with the rules. This study will use the SCCA, Inc. measurement method, so the results can be applied directly to the racecars.

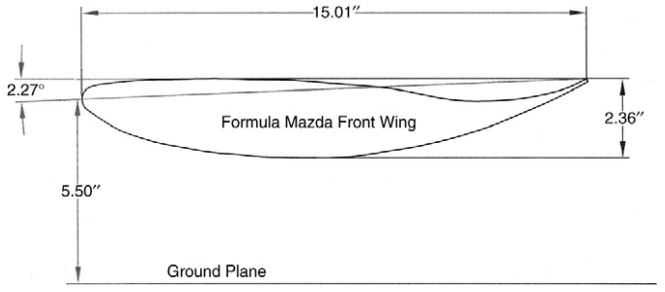

Fig. 2. Cross section drawing of front wing (airfoil).

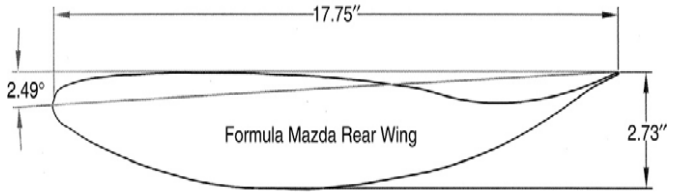

Fig. 3. Cross section drawing of rear wing (airfoil).

3. Physical characteristics of the wings

A Formula Mazda front wing is a single element configuration comprised of two sections, one on either side of a fiberglass nose. Each wing section has angle of attack adjusters on the inboard end and spill plates on the outboard end. The wing has a chord of 15 in. It is mounted with the center of the leading edge 5.5 in. above the ground, well within the distance of ground effect. The simulation here will concentrate on the angle of attack and effect of the ground on the lift and drag in the case of the front wing on the car, and on the effect of the angle of attack on the rear wing. A sectional drawing of the front wing is shown in Fig. 2. The angle dimension in the drawing is the difference in angle of attack between the SCCA, Inc. measurement method and standard aerodynamic practice. Based on the wing dimensions and the properties of Standard Air, the front wing operates at $Re = 0.9 \times 10^6$ at 80 miles/h and at $Re = 1.5 \times 10^6$ at 130 miles/h.

A drawing showing the cross section of the rear wing is shown in Fig. 3. It is of single element design with two support struts in the center and spill plates on the end. Angle of attack adjusters are provided as part of the support strut assembly. The wing has a chord of 17.75 in. (SCCA, Inc). The wing is mounted above the bodywork and can be considered to be in free air. The dimensioned angle in the drawing is the difference in angle of attack between the SCCA, Inc. measurement method and standard aerodynamic practice. Based on the wing dimensions and the properties of standard air, the rear wing operates at $Re = 1.1 \times 10^6$ at 80 miles/h and at $Re = 1.8 \times 10^6$ at 130 miles/h.

4. The physical model

The problem was treated as a two-dimensional problem to validate the concept and to determine the amount of computer resources required for future work. Racecars, on the other hand, generally have a finite depth of airfoil, and hence the treatment here is mainly to capture the main features of the airfoil geometry and the effect of the important parameters such as the angle of attack and the ground effect on the front airfoil Ref. [1] describes limitations of applying two-dimensional wind tunnel results to three-dimensional wings with finite length Refs. [8,9] expanded on this specifically to racecar applications where the flow about the airfoil interacts with the ground and body. Because of this interaction, only a small part of the wing operates in true two-dimensional conditions. Despite these limitations, the two-dimensional approach can be applied to this problem, because the problem is structured as a comparison between different conditions using the same airfoil.

The wings are inverted to create downforce instead of lift. Hence the angle of attack nomenclature is reversed from aerodynamic convention as applied to aircraft. A positive angle of attack means that the leading edge is lower compared to the trailing edge. The front and rear wings were each modeled at −4°, 0°, 4°, 8°, 12°, and 16° angle of attack (AOA). The 16° AOA was chosen as the maximum angle of attack allowed in this study, due to the limitations of the SCCA, Inc. regulations. The −4° AOA was chosen on the other end of the scale because that is physically the adjustment limit of the wings when mounted on the racecar. To see the effects on the front wing in free air, two models with AOA of 0° and 4° were created and studied in this paper.

5. The computer model

The numerical model was set up and run using the Star-CD Computational Fluid Dynamics (CFD) code. Due to the assumption of isothermal flows and no heat transfer, the energy equation was not introduced. This can be justified by the fact that the viscous dissipative term in the energy equation is not expected to be significant, and also by the fact that, more often than not, these wings are painted in light or white colors, as seen in Fig. 1, to reflect any sunlight, maintaining near-ambient temperature conditions on the wing surfaces. The combination of these two effects will minimize any significant temperature changes through the boundary layer and hence negates the necessity to couple the momentum and energy equations due to variable thermal properties as a function of temperature. The continuity and momentum equations remain to be solved. The turbulence was modeled using the k–ε method. The various equations and the default values associated with this turbulence model are discussed in more detail in [10] and are not discussed here.

The front wing is basically attached to the sides of the body of the race car, while the back wing is attached using a strut to the body of the car. These would normally introduce some 3-D effects into the flow patterns developed around these wings. It is expected, though, that the results of the 2-D simulation will be uniformly affected by these construction detail. However, the relative results and trends for the different simulations are expected to stay relatively the same. The mode of attachment for the front wing would most probably create a slight decrease in the negative lift as the air flow speed becomes faster on the top of the wing due to the narrowing of the flow channel as a result of the frontal shape of the body of the race car, while the drag will increase a little due to the increase in the localized velocities around the wing. For the rear wing, there will probably be a minimal change in the lift, because the horizontal cross-section of the strut holding the wing is relatively small, while there would be a small increase in the drag coefficient due to the increased velocity locally as the flow area on the wing near the strut is diminished by that cross-sectional area. Any end effects for either wings, such as vortex generation, are assumed to be relatively small due to the relatively small Reynolds number of the flow.

Ranzenbach [6] suggested dimensions of a calculation grid, placing the leading edge 1.75 times the chord length downstream from the inlet with the outlet located 3 times the chord length downstream from the trailing edge. The suggested distance of the grid above and below the airfoil is 2.56 times the chord. These dimensions were used for this problem. For the 45.05 cm (17.75 in.) rear wing chord, this is calculated as 77.5 cm (31.0 in.) between the inlet and leading edge, 135.25 cm (53.25 in.) behind the trailing edge, and 114.3 cm (45 in.) on the top or bottom of the airfoil. These numbers were rounded off to obtain a rear wing calculation grid of 274.32 cm × 228.6 cm (108 in. long × 90 in. tall). The leading edge of the wing was set at 90.0 cm (36 in.) from the inlet, which meant that the trailing edge was 137.16 cm (54.0 in.) forward from the outlet. The default symmetry boundaries were accepted at the top and bottom as a condition where the normal velocity and normal gradients of all other variables are zero. This was the most suitable of all the boundary conditions offered by Star-CD. For the front wing in ground effect, the height of the grid was modified by a wall boundary 13.97 cm (5.50 in.) below the leading edge to simulate the ground plane.

The calculation grid for the front wing was constructed to include 1764 cells. Fig. 4 shows the grid of the front wing in ground effect. Fig. 5, which has 10,968 cells, shows the grid pattern for the back wing.

A grid independency test was performed on the front airfoil to determine a suitable mesh size for the problem. Three nodal densities were chosen for the runs, i.e. 2208, 4416 and 8832 nodes. Fig. 6 and Table 1 present results to validate the choice of grid density. Fig. 6 shows a plot of velocity profiles on a vertical line chosen at 12.7 cm downstream (horizontally) from the airfoil leading edge. The line spans the distance from the bottom of the airfoil to the ground level. Table 1 also summarizes the values of the integrated F_y downforce on the airfoil. Both these results indicate that there is practically no difference in the overlaid values of the velocity for these three nodal densities, and

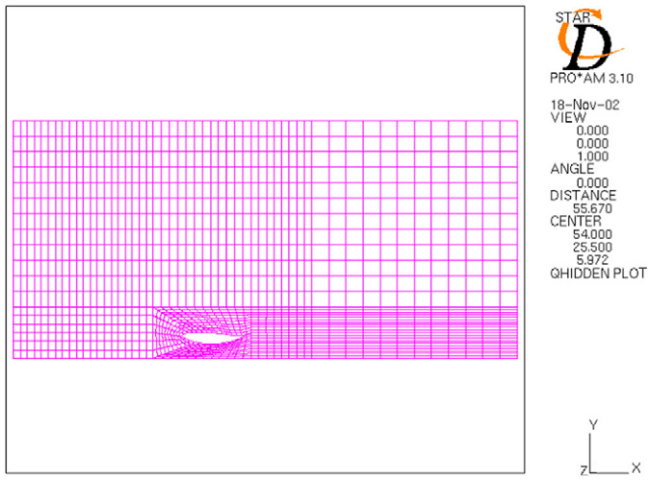

Fig. 4. Front wing in ground effect grid pattern.

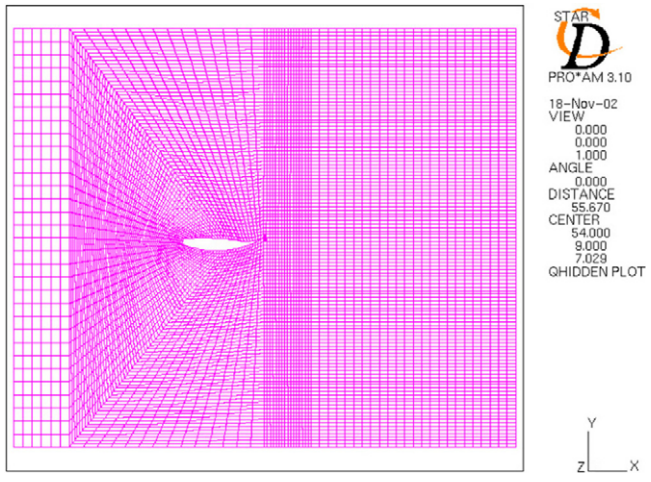

Fig. 5. Rear wing grid pattern.

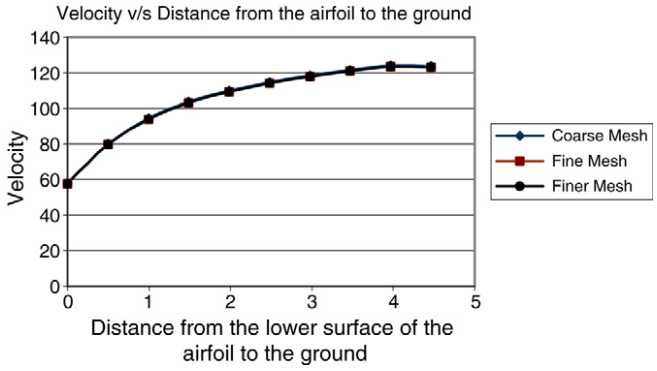

Fig. 6. Grid independency test for numerical problem.

also that there are very small differences between the calculated normal downforce (1.0%), which is deemed accurate for engineering calculations.

Table 1
Additional grid independency calculations using net downward force values

Mesh size	No. of nodes	Downforce Fy (N)
Coarse	2208	961.54
Fine	4416	955.41
Finer	8832	954.498

Table 2
Comparison between airfoil performance in free air and with ground effect

Airfoil in free air		Airfoil with ground effect	
Angle of attack	Downforce (N)	Angle of attack	Downforce (N)
0	642.08	0	808.92
4	848.46	4	961.54

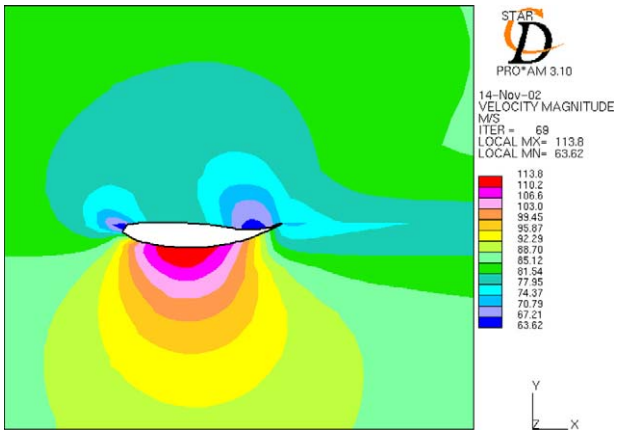

Fig. 7. Front airfoil in free air velocity (0° AOA).

6. Results and discussions

The results of the computer simulations were complied and plotted graphically. The velocity plots show the magnitude of the air velocity at the different points in the flow field. The velocity distribution is normalized using the local velocity to the free stream velocity and plots the resultant values against the normalized chord length for a velocity distribution across the length of the chord. In the same manner, the coefficient of pressure is plotted against the normalized chord to develop a pressure distribution.

6.1. Front wing (airfoil)

Figs. 7 and 8 illustrate the velocities for the front wing operating in a non-obstructed airflow and with the center of the leading edge operating 13.97 cm (5.50 in.) above the ground (with ground effect), respectively. With the airfoil close to the ground, the velocity on the upper surface is slower than for the airfoil in free air. On the lower surface of the wing, the velocity is higher for the airfoil in ground effect than the one in free air using the principle of continuity to maintain the same flow under the wing downstream as the wing upstream.

The following two graphs, Figs. 9 and 10, show that the airfoil in ground effect generates more downforce than the airfoil in free air. Both show a greater pressure difference between the upper surface and the lower surface for the airfoil operating in ground effect than the one operating in free air. The velocity and pressure on the upper surface of the two airfoils show only a little bit of variance. Most of the difference between the two airfoils occurs on the lower surface. Table 2 is a comparison between the airfoils in free air and with ground effect for 0° and 4° angles of attack.

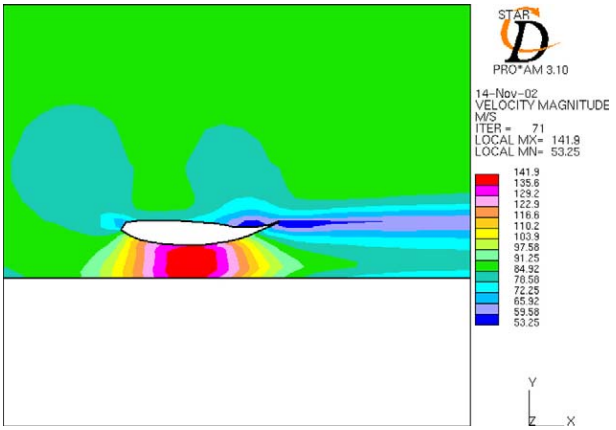

Fig. 8. Front airfoil in ground effect velocity (0° AOA).

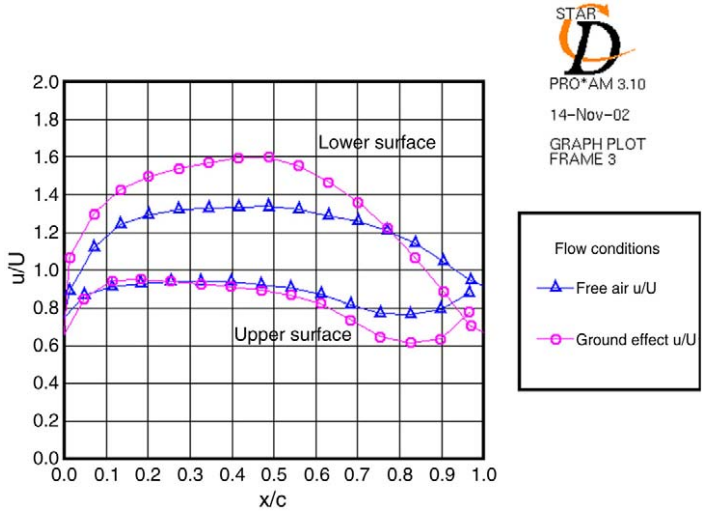

Fig. 9. Free air/ground effect velocity distribution (0° AOA).

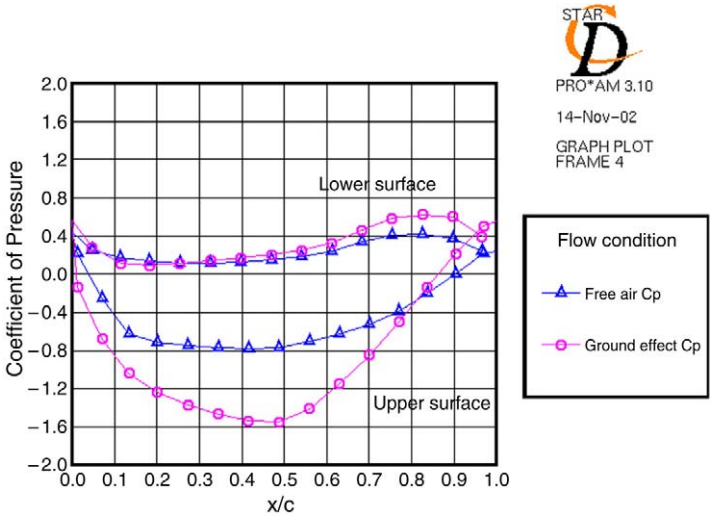

Fig. 10. Free air/Ground effect pressure distribution (4° AOA).

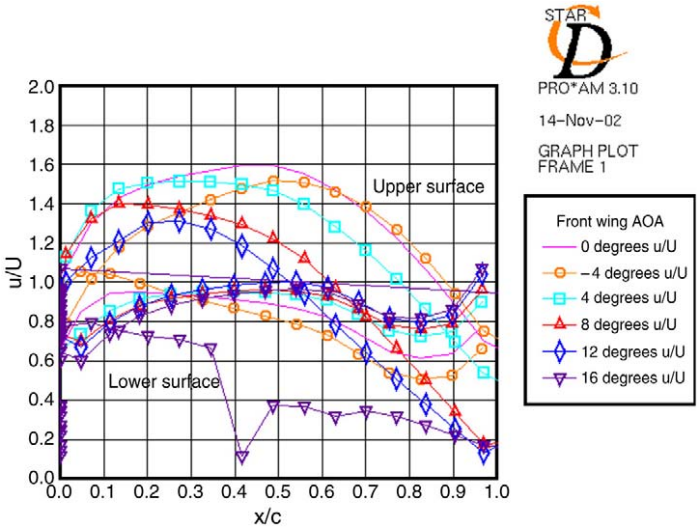

Fig. 11. Front wing velocity distribution with different AOAs.

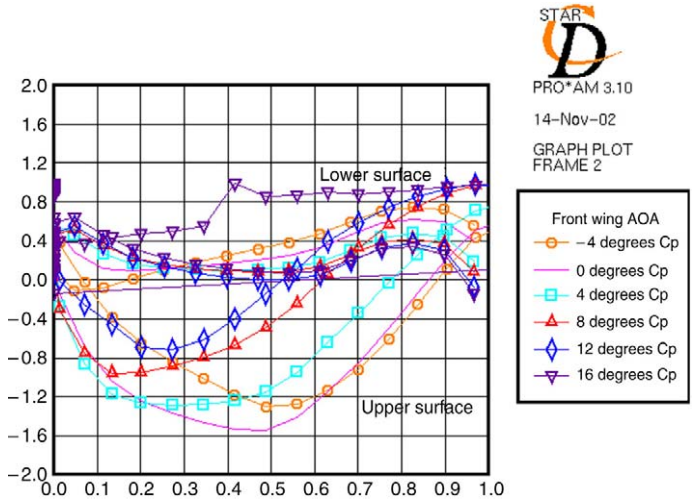

Fig. 12. Front wing pressure distribution with different AOAs. (For interpretation of the references to colour in this figure legend, the reader is referred to the web version of this article.)

Figs. 11 and 12 summarize the results of several runs for the front wing with different AOAs with ground effect. At 12° AOA, the region of high velocity begins to separate from the airfoil surface at the trailing edge. This shows that the airfoil is beginning to approach a "stall condition". At 16° angle of attack, separation occurs at about half the chord length. This is confirmed by the velocity and pressure distributions in those figures. Of interest is the sudden velocity jump downward at around $x/c = 0.4$ for the wing at 16 AOA. This is likely a result of the separation phenomenon. Another observation that was made was the existence of a vortex downstream of the airfoil at this AOA (gray–blue area of Fig. 12).

x is the horizontal dimensional variable starting from the front tip of the wing, while c is the chordal length of the wing horizontally from the upstream tip to the wing's tail. The vertical axes of Figs. 9 and 10 are plots of the non-dimensional u/U and the coefficient of pressure C_p, respectively. u is the horizontal velocity near the wing and U is the freestream horizontal velocity used at the entry to the solution field. The velocity and pressure distributions are similar on the upper surface for all angles of attack. The differences occur in the velocity and pressure distributions on the lower surface. Usually, increasing the angle of attack would increase the downforce. A look at the pressure plots

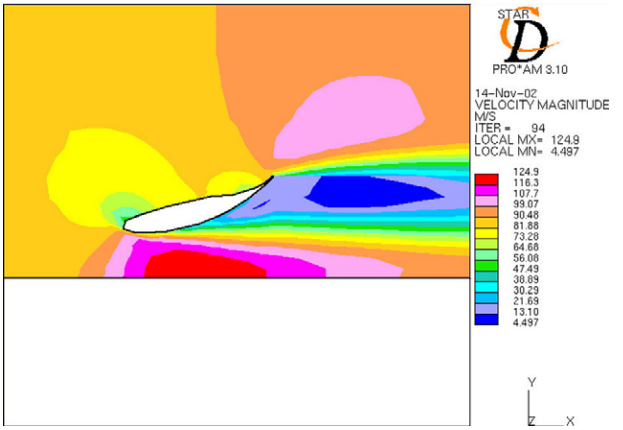

Fig. 13. Front wing velocity distribution with 16° AOA.

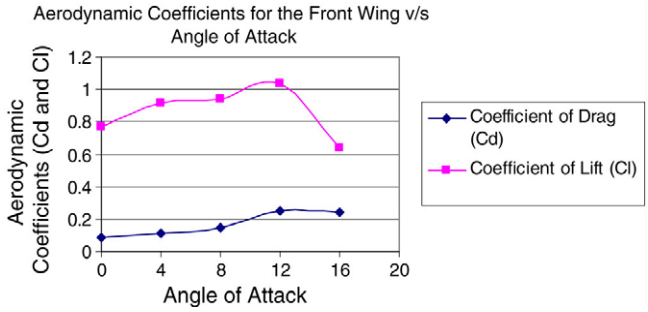

Fig. 14. Front wing variation of the C_d and C_l as a function of AOA.

shows that a greater portion of the lower surface of the wing is in close proximity to the ground. The air accelerates through the gap between the airfoil and the ground, creating a low-pressure area. The greater the portion of the lower surface that is in close proximity to the ground, the larger the low-pressure area and hence, the greater the downward force will be. Fig. 13 represents the plot of the velocity field for the 16° AOA which indicates a fairly high velocity near the ground as opposed to above the airfoil, with some rather low velocities at the trailing edge of it. This latter area indicated some flow reversal for this case as well.

The CFD code is able to calculate the resultant lift and drag force on the wing, and Fig. 14 shows the variation of the coefficients of lift (C_d) and drag (C_l) for various angles of attacks of the front wing in ground effect. The greatest downforce occurs at 12° AOA. This shows the condition of what could be considered the "stalling" condition. The C_d is the normalized (by dividing by the velocity head) and integrated horizontal force on the wing surface area, while the C_l is the normalized (by dividing by the velocity head) and integrated vertical force on the wing area.

6.2. Rear wing

For the rear wing, only the free standing wing airfoil is simulated, as the wing is much higher off the ground and hence no ground effect was simulated for this paper.

Fig. 15 shows a sample velocity plot for the rear wing with 0° angle of attack and indicates, in general, the higher velocity magnitudes on the bottom surface of the airfoil, as expected due to the inverted positioning of these airfoils.

Different cases were run for the other angle of attacks, and the plots obtained were compared with that of 0° angle of attack. Figs. 16 and 17 depict a sample of the variation of the velocity and pressure distribution at 0° AOA, respectively. As expected for the inverted airfoils, the low-pressure suction area is on the lower surface of the airfoil, with the positive pressure side being on the upper surface of the airfoil. Figs. 18 and 19 show sample plots of the contours for two AOAs, showing pressure and velocity plots at 8° and 12° AOA, respectively for the rear wing. Figs. 20 and 21 show the summary of the velocity and pressure normalized distributions for the different angles of

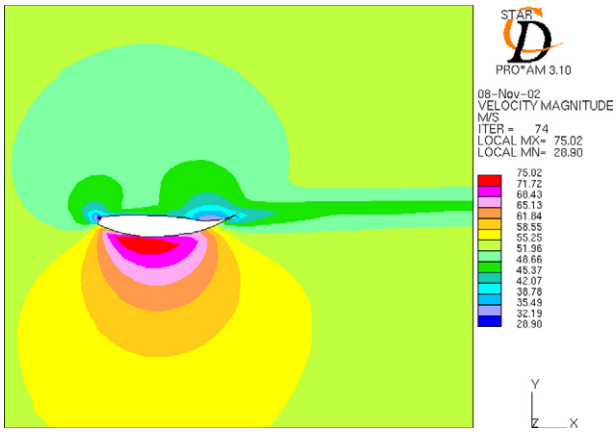

Fig. 15. Rear wing with 0° AOA.

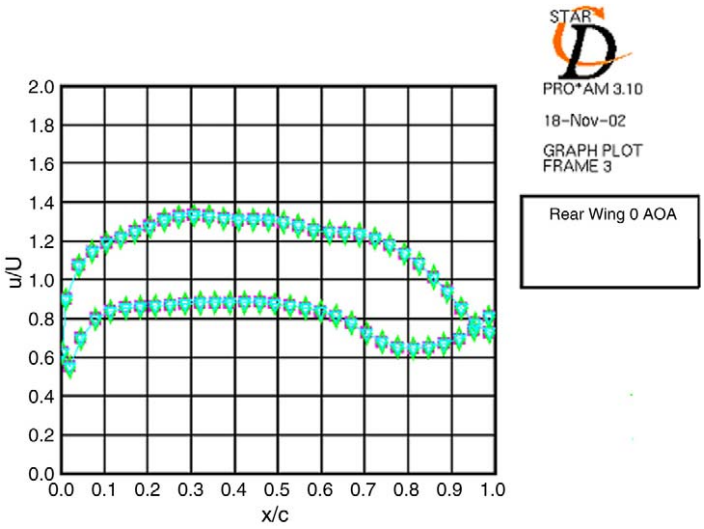

Fig. 16. Rear wing with 0° AOA — velocity distribution.

attack. The velocity takes a drastic downward turn on the lower surface at $x/c = 0.5$ for the airfoil at 12° angle of attack and at $x/c = 0.2$ for the airfoil at 16° angle of attack. The pressure plot shows a drastic dip at $x/c = 0.42$ for the airfoil at 16° angle of attack. The appearance of stalling can be observed clearly. For the rear wing, the stalling starts just after 8°.

Fig. 21 shows the profiles of pressure, normalized as the coefficient of pressure on the different wing locations. Some of the values observed in this figure are negative on the lower surface between 0.0 and −0.8, which indicate, as expected, the correctly intended wing operation in creating a negative lift from the airfoil geometry so as to help more in keeping the vehicle on the track. However, with the increase in the low-pressure area at the trailing edge, there is an increase in drag. As the angle of attack is increased to 12° and 16°, the high-pressure area increases on the upper surface, but it also moves forward, again increasing drag. At 12° angle of attack, the area of high velocity begins to separate from the airfoil surface (see Fig. 20). This shows that the airfoil is beginning to approach a stall condition. On the velocity plot at 16° angle of attack, the separation point can be seen to moving forward. As with the front wing at 16° angle of attack, a vortex is observed from the detailed vector plots (Fig. 19) in the wake of the trailing edge.

Fig. 22 plots the variation of the coefficients of lift C_d and drag C_l for various angles of attacks of the rear wing. The greatest downforce occurs at 12° angle of attack. This shows the beginning of the condition of “stalling”.

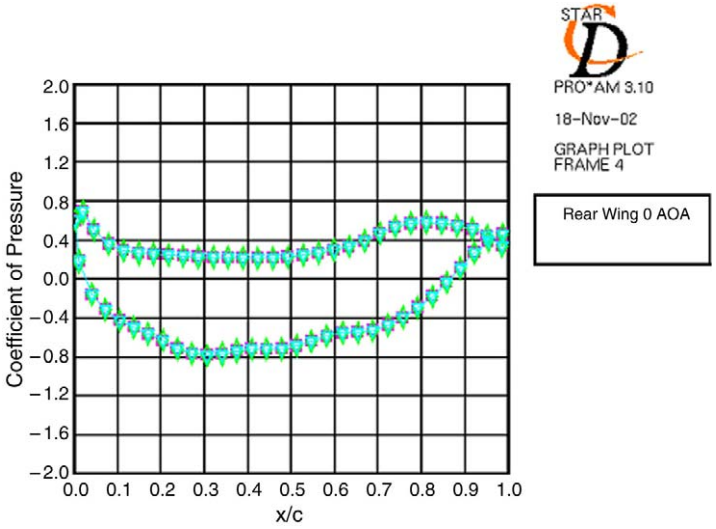

Fig. 17. Rear wing with 0° AOA — pressure distribution.

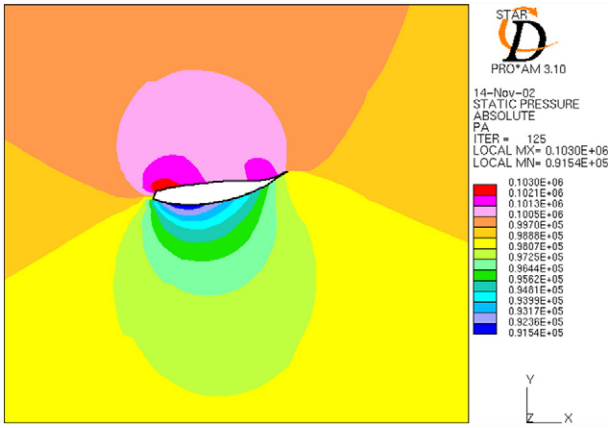

Fig. 18. Rear wing with 8° AOA — pressure plot.

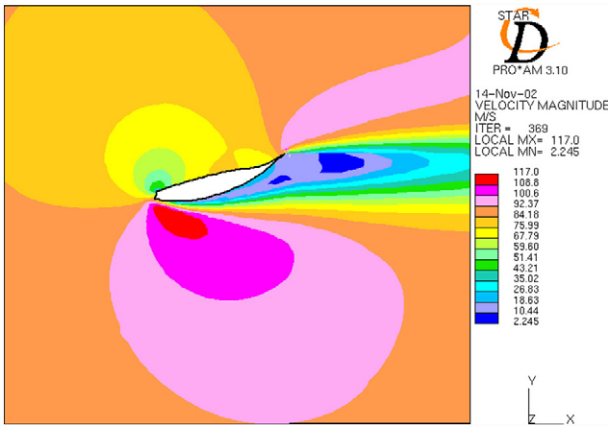

Fig. 19. Rear wing with 16° AOA — velocity plot.

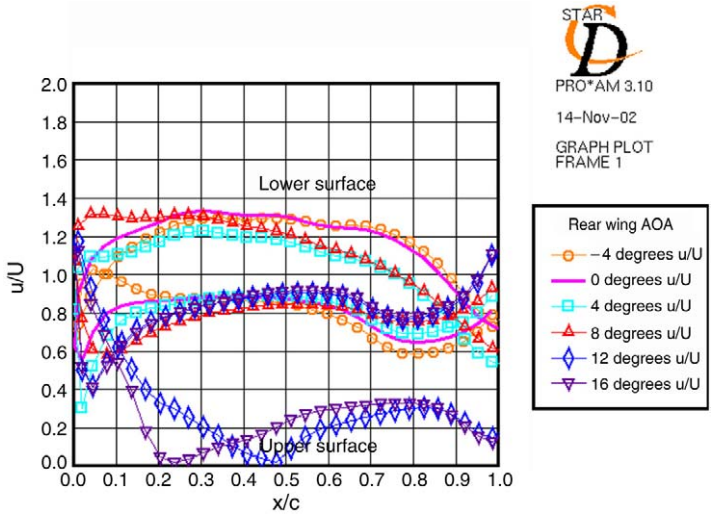

Fig. 20. Rear wing with different AOAs — velocity distribution.

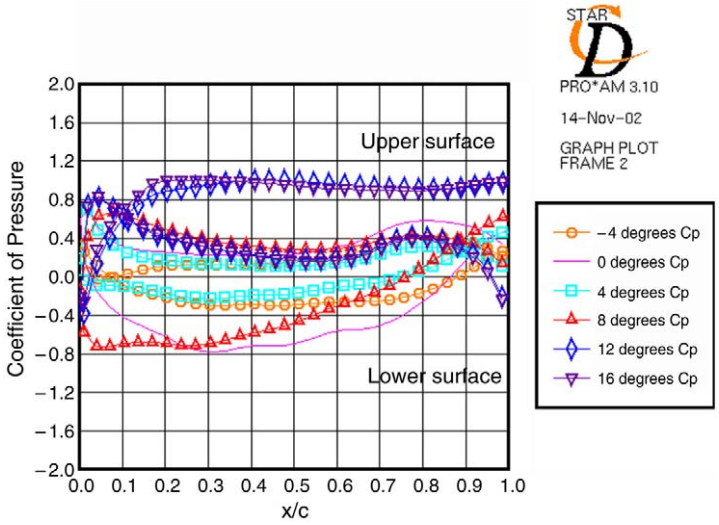

Fig. 21. Rear wing with different AOAs — pressure distribution.

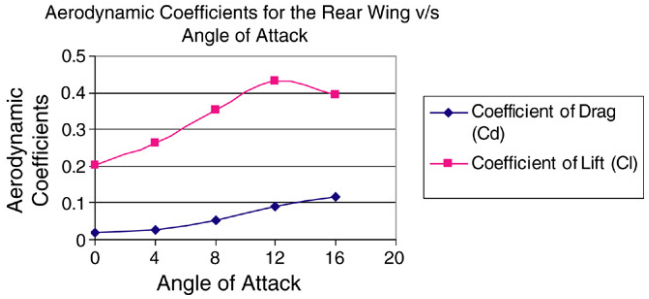

Fig. 22. Rear wing variations of the coefficient of drag and lift C_d and C_l as a function of AOA.

7. Discussion and conclusions

A two-dimensional CFD study has been performed on the airfoil profiles of the front (with/without ground effect) and rear wings (free standing) of a Formula Mazda race car for various AOA. Detailed velocity and pressure distribution plots along the surfaces of the airfoils have been presented. As suspected, the front wing's performance seems to be affected by the existence of the ground nearby. The front wing seems to develop a larger net downforce (negative lift) when flow is simulated with ground effect. This can be seen through the marked increase in negative pressure shown in Fig. 10 due to that effect. Table 2, shown earlier, presents the effects of the ground on the downward lift for AOAs 0° and 4°. The calculated results clearly show an increase in this force when a front airfoil is considered with ground effect of about 13% to 20%. This increase can be attributed to the anticipated velocity increase on the underside of the wing, which in turn decreases the pressure on the wing from that side. Fig. 14 summarizes the results of the coefficients when ground effect is considered, and shows that there is a slight increase in the C_l of about 20% from 0° to 12° AOA. In addition, there is a marked decrease in C_l by about 45%, which may indicate that between 12° and 16° AOA there is a potential for a "stall" condition with the airfoil. Also, the C_d for this wing shows a steady increase to about 50% until the 12 AOA is reached, after which the value of the coefficient value becomes relatively constant. This is anticipated to be the case where increased drag is achieved on the wing, along with the increased lift, until the expected stall condition is approached.

When considering the rear wing airfoil, Fig. 22 indicates a similar effect on the front wing and shows the marked change in the C_l as the AOA approaches 12°. After this, there is a drop in that value of about 10%, indicating the suspected "stall" condition. In a similar vein, there is a marked monotonous increase in the C_d as the AOA increases, which is anticipated with these types of wings.

These results indicate that, for design purposes, consideration of the front airfoil has to be taken with the effect of the ground for the proper overall consideration of the stability and handling of the Mazda race car. For both airfoils, the hydrodynamic performance of the foils are significantly affected by the AOA and need to be considered for the overall handling of the car. These values, along with experimental validation and an overall analysis of the forces on the particular steering mechanisms of these race cars, and along with race track conditions, can enhance the optimum handling of these vehicles.

Future work is suggested to perform parametric studies of various ground clearances of the front foil to see its effect on the aforementioned coefficients. Also, the consideration of the thermal temperature gradients around the race car and its effects through the air density on these coefficients should be studied.

References

[1] Ira H. Abbott, Albert E. Von Doenhoff, Theory of Wing Sections, Dover Publications, Inc., New York, 1959.
[2] Robert Liebeck, Design of subsonic airfoils for high lift, AIAA Journal of Aircraft 15 (9) (1978) 547–561.
[3] Richard Eppler, Airfoil Design and Data, Springer-Verlag, Berlin, Heidelberg, Germany, 1990.
[4] Dan H. Neuhart, Odis C. Pendergraft Jr., A Water Tunnel Study of Gurney Flaps, National Aeronautics and Space Administration, NASA Technical Memorandum 4071, 1988.
[5] Joseph Katz, Lee Dykstra, Effect of Wing/Body Interaction on the Aerodynamics of Two Generic Racing Cars, Society of Automotive Engineers, SAE Paper 920349, Warrendale, PA, 1992.
[6] Robert Ranzenbach, Jewel B. Barlow, Two-Dimensional Airfoil in Ground Effect, An Experimental and Computational Study, Society of Automotive Engineers, SAE Paper 942509, 1994.
[7] Roy Myose, Michael Papadakis, Ismael Heron, Gurney flap experiments on airfoils, wings, and reflection plane model, AIAA Journal of Aircraft 35 (2) (1998).
[8] Joseph Katz, Lee Dykstra, Application of Computational Methods to the Aerodynamic Development of a Prototype Race Car, Society of Automotive Engineers, SAE Paper 942498, Warrendale, PA, 1994.
[9] Joseph Katz, Race Car Aerodynamics-Designing for Speed, Robert Bentley Publishers, Cambridge, MA, 1995.
[10] CD Adapco Group, Methodology, Star-CD, Computational Dynamics Limited, Melville, NY, 1999.